A fungal family of lytic polysaccharide monooxygenase-like copper proteins

Aurore Labourel[1], Kristian E. H. Frandsen[1,2], Feng Zhang[3], Nicolas Brouilly[4], Sacha Grisel[1], Mireille Haon[1], Luisa Ciano[5], David Ropartz[6], Mathieu Fanuel[6], Francis Martin[3], David Navarro[1], Marie-Noëlle Rosso[1], Tobias Tandrup[2], Bastien Bissaro[1], Katja S. Johansen[7], Anastasia Zerva[1,8], Paul H. Walton[5], Bernard Henrissat[9,10,11], Leila Lo Leggio[2], Jean-Guy Berrin[1,*]

[1]INRA, Aix Marseille Univ., Biodiversité et Biotechnologie Fongiques (BBF), UMR1163, F-13009 Marseille, France

[2]Biological Chemistry Section, Department of Chemistry, University of Copenhagen, 2100 Copenhagen Ø, Denmark

[3]INRA, UMR1136, Université de Lorraine 'Interactions Arbres/Microorganismes', Laboratoire d'Excellence ARBRE, Centre INRA-Lorraine, F-54280 Champenoux, France

[4]Aix Marseille Univ., CNRS, IBDM, Marseille, France

[5]Department of Chemistry, University of York, York, UK, YO10 5DD

[6]INRA, Unité de Recherche Biopolymères Interactions Assemblages (BIA), F-44316 Nantes, France

[7]Department of Geosciences and Natural Resource Management, University of Copenhagen, 2100 Copenhagen Ø, Denmark

[8]Biotechnology Laboratory, School of Chemical Engineering, National Technical University of Athens, Zografou Campus, Athens 15780, Greece

[9]INRA, USC1408 Architecture et Fonction des Macromolécules Biologiques (AFMB), F-13009 Marseille, France

[10]Architecture et Fonction des Macromolécules Biologiques (AFMB), CNRS, Aix-Marseille Univ., F-13009 Marseille, France

[11]Department of Biological Sciences, King Abdulaziz University, Jeddah, Saudi Arabia

*Correspondence and materials request should be addressed to J.G.B.

(jean-guy.berrin@inra.fr)

Abstract

Lytic polysaccharide monooxygenases (LPMOs) are copper-containing enzymes that play a key role in the oxidative degradation of various biopolymers such as cellulose and chitin. While hunting for new LPMOs, we identified in various fungal lineages a new family of proteins, defined herein as X325. The X325 three-dimensional structure revealed an overall LPMO fold and a histidine-brace with an additional aspartate ligand to Cu(II). Although LPMO-type activity of X325 members was initially expected, we demonstrated that X325 members do not perform oxidative cleavage of polysaccharides, establishing that X325s are not LPMOs. Investigations of the biological role of X325 in the ectomycorrhizal fungus *Laccaria bicolor* revealed exposure of the X325 protein at the interface between fungal hyphae and tree rootlet cells. Our results provide insights into a family of copper-containing proteins widespread in the fungal kingdom, which is evolutionarily related to LPMOs but has diverged to biological functions other than polysaccharide degradation.

Introduction

The discovery of lytic polysaccharide monooxygenases (LPMOs) has overturned much of the accepted thinking within the field of cellulose and chitin degradation[1-3]. LPMOs are copper-dependent enzymes that break down polysaccharides through an oxidative mechanism involving an electron donor and molecular oxygen or H_2O_2[1,2,4]. LPMOs active on cellulose are able to boost the activity of cellulases to such an extent that they are now incorporated in industrial enzyme mixtures for the conversion of agricultural residues to biofuels[5]. At the active site of LPMOs, the copper ion is bound through a histidine brace, which comprises a N-terminal histidine that chelates a single copper ion through its amino terminus -NH_2 and the Nδ of its imidazole side chain. This N-terminal histidine residue is usually methylated by filamentous fungi[2,6] and, although recent studies have suggested a role in protecting the enzyme from self-oxidative inactivation[7], the function of this modification is yet to be fully elucidated. The copper coordination is completed by the Nε of an additional histidine side chain, to form an overall N_3 T-shaped geometry[8].

The recently discovered LPMO families have been identified by a "module walking" approach. This method relies on the fact that many CAZymes are multi-modular with one or more additional domains, which are often substrate-targeting carbohydrate binding modules (CBMs)[9]. The modules attached to known CAZymes were used to search for proteins, which (i) contained those modules, (ii) contained a conserved histidine immediately after the signal peptide cleavage site and (iii) displayed insignificant sequence similarity to known AA9 and AA10 families. This method has led to the discovery of several LPMO families (AA11[10], AA13[11,12], AA15[13]) but does not allow the identification of new LPMOs lacking additional modules. In a complementary approach based on comparative post-genomic analyses applied to fungal saprotrophs, we recently identified xylan-active AA14 LPMOs[14] and cellulose-

active AA16 LPMOs[15]. These examples emphasized the fact that fungal secretomes are a promising ground to hunt for new LPMOs and to gain insights into their biological role[16].

Using a similar approach, here we report the discovery of a widespread copper-containing protein family, named X325, found in various fungal lineages including saprotrophic and ectomycorrhizal (ECM) fungi and yeasts. Although X325 family members share many structural features and a probable common ancestor with biomass-degrading LPMOs, their copper binding site is atypical and more similar to the ones of other copper-binding proteins involved in copper homeostasis. This study reveals new prospects for LPMO-like proteins with biological functions other than polysaccharide degradation.

Results

Discovery of the X325 family

The basidiomycete *Laetisaria arvalis* (strain BRFM514) is able to grow on cellulose or wheat straw as the sole carbon source and to fully digest cellulose filter paper[17]. Global transcriptome and secretome analyses revealed that *L. arvalis* produces a unique repertoire of CAZymes, including a complete set of cellulose-acting enzymes[17]. Searching for proteins with predicted N-terminal histidine among *L. arvalis* post-genomic data led to the identification of a protein of unknown function (GenBank ID MK088083, here termed "*La*X325") that was secreted during growth on cellulose and wheat straw. In-depth analysis of the proteomic data obtained from the *L. arvalis* secretome revealed that the N-terminal histidine is methylated (mass +14.0157 Da), a feature commonly observed in fungal LPMOs[2]. Moreover, a protein fold recognition analysis[18] using X325 as a template matched the cellulose-active AA10 LPMO from *Streptomyces coelicolor* (PDB code 6F7E[19]) with 97% confidence but only 14% sequence identity. This level of sequence relatedness is however insufficient to group X325 with the bacterial LPMOs that mostly compose family AA10. Therefore, X325 was used as the query sequence for a BLAST search on the non-redundant protein sequence database of the NCBI database, and this retrieved approximately 550 significantly related sequences (e-values lower than 4×10^{-4}). Alignments of the retrieved sequences (**Supplementary Figure 1**) showed two conserved histidine residues, one being the N-terminal of the mature protein, compatible with a copper-binding histidine brace[2], a hallmark of all known LPMOs. Interestingly, none of the X325 sequences carries a CBM but instead invariably harbor a glycosylphosphatidylinositol (GPI) anchor at the C-terminus (**Supplementary Figure 1**). Usually, proteins attached to a GPI anchor via their carboxyl terminus are found in the outer leaflet of the lipid bilayer facing the extracellular environment[20]. GPI-anchors can also be considered as predetermined breaking points that

allow the release of proteins into the extracellular environment upon enzymatic cleavage[20]. Such a release of the protein from the membrane could explain the presence of *La*X325 in the secretomes of *L. arvalis*[17]. The phylogenetic analysis of X325 modules (conducted after removal of signal peptides and GPI anchors) was performed on 123 protein sequences encoded by 58 genomes selected to represent the fungal diversity (**Figure 1**). The analysis shows that X325 proteins are present across the fungal kingdom including early-diverging fungi within Mucoromycotina[21], saprotrophic fungi, symbiotic fungi, endophytic fungi, plant/animal pathogens and, more surprisingly, several yeast species lacking plant cell wall-degrading enzymes. This was an indication that X325s may have a different function than oxidative cleavage of glycoside linkages in plant biomass. The phylogenetic tree of X325 members shows that the family is divided into six distinct clades, two only gathering basidiomycetes and the four other ones only ascomycetes (**Figure 1**). On average 2.3 X325-encoding genes are found per fungal species.

Based on the X325 phylogenetic analysis, we selected several X325 candidate genes from different clades/subgroups (**Figure 1**) within model fungi/yeasts and recombinantly expressed them in *Pichia pastoris* (**Supplementary Table 1**). Using this method, we produced and purified four X325 proteins: *La*X325 from the fungal saprotroph *Laetisaria arvalis* (GenBank ID MK088083), *Pa*X325 from the coprophilous fungus *Podospora anserina* (GenBank ID XM_001907524.1), *Lb*X325 from the ECM fungus *Laccaria bicolor* (GenBank ID XM_001874260.1) and *Yl*X325 from the yeast *Yarrowia lipolytica* (GenBank ID XM_505821.1). The correct processing of the native signal peptide, which exposed the N-terminal histidine residue at position 1 in the mature polypeptide chain was confirmed using N-terminal sequencing. ICP-MS analyses revealed that recombinant X325 proteins contained approximately one copper atom per protein molecule.

X325 crystal structure displays a fold similar to LPMOs

The three-dimensional structure of *La*X325 was solved by single-wavelength anomalous dispersion (SAD) phasing at the copper edge, and refined in three crystal forms at resolutions around 2 Å (**Supplementary Table 2**). The core of the protein folds into a largely antiparallel immunoglobulin-like β-sandwich, a fold similar to that seen in LPMO structures[22] (**Figure 2a**). The closest structural homologue in the PDB90 database according to the DALI-server[23] is the recently determined *Thermobia domestica* AA15 LPMO structure (**Supplementary Figure 2**; PDB 5MSZ, Z-score of 11.0), closely followed by four bacterial AA10 LPMOs (5FJQ, 2BEM, 5WSZ and 5L2V). Two conserved disulfides (formed by Cys22/Cys128 and Cys93/Cys145) stabilize the *La*X325 structure (**Supplementary Figure 1**). However, unlike LPMOs implicated in polysaccharide degradation, X325 lacks extended binding surface capable of accommodating polysaccharide substrates. This can be highlighted by comparison with *Ls*AA9A in complex with cellohexaose (**Figure 3a**). Furthermore, the GPI anchor would protrude from the face of the protein expected to bind polysaccharides (**Figure 3a**) and no conservation of residues typically associated with polysaccharide binding is observed on the surface of X325 near the copper binding site (**Supplementary Figure 3**).

X325 structure reveals an unusual copper binding site

In addition to the overall folding similarity in the structure of *La*X325 to *bona fide* LPMOs, the canonical histidine brace coordination formed by two histidines (His1 and His49) is preserved and the second histidine is found in a loop topologically equivalent to that holding the second histidine in structurally-characterized LPMOs, although the angle between the two imidazole planes is somewhat different than usually observed[8] (**Figure 2b**). A tyrosine (Tyr118) is present below the copper equatorial plane, but on a topologically different strand to that commonly found in e.g. AA9 LPMOs. Although tyrosine residues within or close to

159 axial coordination distance to the copper binding site are a common feature in many LPMOs,
160 in the *La*X325 structures this tyrosine residue is positioned away from the metal ion (average
161 Cu-O distance = 4.6 Å; **Figure 2b**). Furthermore, this tyrosine is not conserved across the
162 X325 family (**Supplementary Figure 1**).
163
164 In striking contrast with known LPMOs, the copper is further coordinated by an aspartate side
165 chain (Asp122, average Cu-O = 2.0 Å), in its flat equatorial plane. The second oxygen atom
166 of the carboxylate of the aspartate side chain lies below the flat equatorial plane of the copper
167 at an average Cu-O distance of 2.9 Å. Above the plane, density identified as a fully occupied
168 water molecule is present in the axial position of the copper coordination sphere in both the
169 $P2_1$ and the $P2_12_12_1$ crystal structures in four out of six independent molecules. The geometry
170 of the Cu in terms of θ1, θ2 and θ3 angles falls mostly within the values usually observed for
171 Cu(II) in LPMOs[24] (**Supplementary Table 3**).
172
173 A similar copper coordination in the three crystal forms confirms Asp122 as copper ligand.
174 Asp122 is located in a semi-conserved GGDGN loop equivalent to loop 8 in AA9 LPMOs[22].
175 Based on its amino acid composition, the loop is likely to be flexible and perhaps move in
176 response to a transition to Cu(I), but no conformational change was observed in the crystals
177 treated with 5 mM L-cysteine or extensively exposed to X-rays.
178
179 Asp is not an unprecedented ligand for copper in metalloproteins. In fact, such coordination
180 by a carboxylate is seen for LPMOs both in fusolin[25] (belonging to the AA10 family, PDB
181 4YN2, 4OW5, 4X27 and 4X29) and *Nc*AA9F[26] (PDB 4QI8) (**Supplementary Table 3**)
182 crystals, but *only in the crystal*, as the Glu/Asp comes from a symmetry-related molecule.
183 Additionally, the copper binding protein CopC[27] (**Figure 2b**, **Supplementary Table 3**) has a

structurally similar binding site with a His brace and an Asp coordinating copper, although the atomic arrangement is not identical since the Asp and one His have swapped position and the imidazole Nδ is coordinating the copper (rather than Nε as in canonical LPMOs). Very recently, it has been proposed that the true active site in particulate methane monooxygenase (pMMO) is found in the C subunit (Cu_C site), in which two histidines and one aspartate coordinate a copper ion (PDB 3RFR and 3RGB), previously interpreted as a zinc in a tetrahedral configuration not involving the N-terminus NH_2 of the polypeptide[28,29] and thus quite different from both LPMOs and X325. Sequence alignments of X325 members showed that the *La*X325 Asp122 is mainly conserved across the family, but - in an important variation - a subgroup displays a histidine in this position instead (**Figure 1b**; **Supplementary Figure 1**). The copper binding site arrangement in this subgroup could thus appear to be very similar to that seen in the N-terminal copper binding site (Cu_B site) of pMMOs (**Figure 2b**; **Supplementary Figure 2**) originally believed to be the active site but now challenged[28,30].

X325 proteins are spectroscopically similar to LPMOs

Continuous wave (cw) Electron Paramagnetic Resonance (EPR) spectroscopy was carried out on *La*X325 to investigate the copper active site of this protein (**Figure 2c**) for which the 3D structure was available. The spin Hamiltonian parameters determined from the simulations of the X band spectrum (**Figure 2c** and **Supplementary Table 4**) showed that the active site of *La*X325 falls within a type 2 classification[31], with $g_z = 2.260$ and $|A_z| = 543$ MHz. Due to the presence of the His-tag, which could potentially offer a competitive binding site for the copper, a careful Cu titration was performed (**Supplementary Figure 4**). This titration reveals that the only observable copper species in the EPR spectra derives from the metal bound at the histidine brace active site, if no excess copper is present. The spin Hamiltonian parameters, with a $d(x^2-y^2)$ SOMO, are similar to those obtained for LPMOs, suggesting that

the presence of the coordinating Asp residue does not substantially affect the coordination environment of the active site.

X325s proteins are not LPMOs

To assess whether the four different X325 proteins recombinantly produced are able to act on polysaccharide substrates in an LPMO-type manner, we performed activity assays on a wide range of plant cell wall polysaccharides including cellulose, xylan, xyloglucan, (1→3)-(1→4)-β-D-glucan, glucomannan, pectins and soluble oligosaccharides and on fungal cell wall polysaccharides including chitin, chitosan, β-(1→3) glucan, β-(1→6) glucan, and a fungal cell wall extract from *L. bicolor*. No substantial level of oligomeric products was detected by ionic chromatography except when cellulose was used as substrate, in which case small soluble cellooligosaccharides peaks were detected concomitantly with barely detectable peaks eluting at the same retention time as C_1-oxidized peaks. Although the oxidative nature of these C_1-oxidized peaks were confirmed by mass spectrometry (**Supplementary Figure 5**), their abundance was negligible compared to the copper control condition and to a cellulose-active AA9 LPMO[6] that produced large amount of C_1-oxidized products (**Figure 3b)**. In an attempt to explore the reactivity of the X325 proteins and trigger the formation of oxidized products, other enzyme assays conditions were attempted.

Recent reports have proposed hydrogen peroxide as an alternative co-substrate[4,32,33], but addition of H_2O_2 to X325 enzyme reactions had no effect on the product released from cellulose. In the case of family AA9 LPMOs, it is well-established that LPMOs can receive electrons from an external reducing agent (ascorbate, cysteine, lignin, etc.) or from cellobiose dehydrogenase (CDH)[34,35]. Attempts to use either (i) lignin fractions extracted from wood, (ii) duroquinol, which is used as reducing agent for pMMOs[36], or (iii) *P. anserina* CDH under the

experimental conditions used for AA9 LPMOs[22] did not trigger the formation of soluble products. Additionally, mutagenesis work in *Yl*X325 aiming at shortening the side chain of Asp116 (equivalent to Asp122 in *La*X325) to a serine residue (D116S mutation) or replacing the aspartate by its pMMO analogue (D116H) led to the same product profile as the wild type *Yl*X325 (i.e. no activity; **Supplementary Figure 5**), suggesting that the apparent lack of cellulolytic activity is not due to copper coordination by the Asp side chain. To evaluate whether X325 displayed any monooxygenase activity on cellulose, experiments were carried out in the absence of oxygen with and without addition of H_2O_2 (**Supplementary Figure 5**). The release of cellooligosaccharides was neither oxygen- nor H_2O_2-dependent meaning that the presence of cellooligosaccharides was probably due to unspecific binding of X325 proteins to cellulose as already shown for bovine serum albumin (BSA) that causes an increase in soluble reducing ends production[37].

Localization of *Lb*X325 in *Laccaria bicolor*

The *Lb*X325-encoded gene is upregulated during *Laccaria-Populus* ectomycorrhizae formation and a similar trend was also observed for some X325 orthologs in some other symbiotic fungi (**Supplementary Table 5**). In nature, trees rely on ectomycorrhizal symbiosis to acquire the scarce nutrients available in soils[38]. It is widely accepted that ectomycorrhizal fungi have an extremely reduced enzyme portfolio to degrade plant cell walls as their symbiotic plant partner provides them with carbon. Fungal hyphae penetrate the tree rootlets intercellularly to differentiate a hyphal network, the so-called Hartig net[39]. Although Hartig net development does not lead to substantial change in cell wall composition, subtle alterations, such as localized plant cell wall loosening and swelling accompany the hyphal ingression[40,41]. Therefore, we performed immunolabelling experiments on ECM from *L. bicolor* hyphae colonizing *Populus* roots to localize *Lb*X325 and gain insights into its function *in vivo*. To do so, polyclonal antibodies were raised against the purified recombinant

protein *Lb*X325 and their specificity was first assessed by western blot on *L. bicolor* ECM crude extracts (**Supplementary Figure 6**). A strong signal corresponding to the *Lb*X325 molecular weight was detected in the fraction containing the membrane bound proteins. This experiment supported the fungal cell wall localization of *Lb*X325 predicted by the presence of the C-terminal GPI anchor. On ECM sections, anti-*Lb*X325 antibodies led to an intense labeling of hyphae constituting the mantle and the Hartig net (**Figure 4**). Labeling was mainly detected at the periphery of the hyphae and coincided with the location of cell wall chitin labeled by wheat germ agglutinin (WGA), supporting a cell wall and/or apoplastic localization. In the presence of exogenously-added recombinant *Lb*X325 (competitive assay), the specific binding of antibodies to X325 produced *in vivo* by *L. bicolor* was precluded and no signal was detected, confirming the high specificity of the immune serum (**Supplementary Figure 7**). No signal in the *L. bicolor* free-living mycelium (FLM) was detected using confocal miscroscopy (**Supplementary Figure 7**), consistent with *Lb*X325 transcripts being present at low level. For a better resolution, immunogold labelling was also performed on FLM and ECM and transmission electronic microscopy confirmed the fungal cell wall localization of *Lb*X325 (**Figure 4**). A quantitative assessment indicated a preferential localization of *Lb*X325 within and beyond the outer layers of the cell wall, consistent with a GPI anchor that can be cleaved off (**Supplementary Figure 8; Supplementary Table 6**). Thus, the upregulation of the *Lb*X325 gene in ECM compared to free-living mycelium, coupled to its localization, could suggest the involvement of *Lb*X325 in fungal cell wall remodeling during *Laccaria-Populus* symbiosis.

Discussion

The newly discovered X325 family shares several features with LPMOs, which initially led us to expect LPMO activity from proteins of this family. Indeed, like AA9 LPMOs, (i) X325-

encoding genes are upregulated and X325 proteins are secreted by fungi in a plant cell wall modification/degradation context, (ii) X325 proteins harbor two strictly conserved histidine residues, one being at the N-terminal position and methylated *in vivo*, (iii) X325s are monocopper-containing proteins with an overall structural fold similar to LPMOs, and (iv) the coordination by a histidine brace of the copper ion is spectroscopically similar to AA9 LPMOs and geometrically very similar to LPMOs in general. However, X325 members invariably harbor a GPI anchor at the C-terminus. This feature is generally absent in fungal LPMOs. Only a subgroup of AA16 LPMO members displays this C-terminal anchor[15]. GPI-anchored proteins are often involved in biological processes such as cell wall remodeling or transmembrane signaling[42-44]. The GPI moiety can be cleaved off by specific phospholipases, releasing the protein into the extracellular matrix and thus adding a supplemental level of regulation. Furthermore, no substantial oxidative activity could be detected on tested polysaccharides, in good agreement with the analysis of the *La*X325 crystal structure. Indeed, *La*X325 does not display an extended flat binding surface as described in AA9 LPMOs, and no conserved aromatic residues that could promote polysaccharide binding are found in the vicinity of the copper binding site. From a molecular point of view, the *La*X325 crystal structure reveals the presence of an aspartate as the third ligand in the equatorial plane of the copper coordination sphere. As it has been proposed that LPMOs activate oxygen species at the free equatorial site, this could explain the lack of monooxygenase activity for X325 members but mutation of the aspartate residue (equivalent to Asp122 in *La*X325) did not lead to any detectable polysaccharide-degrading activity. Interestingly, some of the X325s display a histidine in place of the *La*X325 Asp122, drawing a parallel with the pMMO Cu_B site, which has been recently proposed not to be the site of O_2 activation for the oxidation of methane[28,29]. Notwithstanding the now apparent lack of oxidative activity of this site in pMMO, the single copper ion is coordinatively saturated in the equatorial coordination plane

similarly to the copper site in X325. This saturation removes an obvious site for O_2 activation, thus indicating that oxidase activity does not occur either at the pMMO Cu_B site or in X325 proteins. What the role of the copper site has in each of these enzymes is therefore not clear, but the obvious parallels between the two would suggest that X325 could contribute to an overall oxidase activity in conjunction with other yet-to-be-discovered partners.

The coordination of copper in *La*X325 is also similar to the Cu(II) site found in the periplasmic copper binding protein CopC, which is believed to play a role in bacterial copper homeostasis[27]. The unusual copper binding site similar to copper binding proteins, associated to the absence of oxidative activity on polysaccharides and the conspicuous lack of CBMs, pose questions about the *in vivo* activity/role of X325 proteins. Copper is required in multiple redox-active enzymes such as cytochrome c oxidases, multicopper oxidases (MCOs), or Cu/Zn superoxide dismutases and, of course, LPMOs in which the redox-cycling of the metal through its Cu(I)/Cu(II) oxidation states is an essential feature of the mechanistic chemistry, especially in reactions with O_2 and/or H_2O_2. In the same regard, an excess of copper is also implicated in the oxidation of proteins and damage to membrane lipids and DNA. Indeed, the uncontrolled activation of O_2 or H_2O_2 by reduced transition metals leads to harmful reactive oxygen species. This dual effect forces organisms to maintain a precise copper homeostasis to enable protein function whilst avoiding metal toxicity[45,46]. From this point of view, in ECM fungi, metal transporters, especially those related to Cu trafficking, display the highest expression levels in mycorrhizae, suggesting extensive translocation of copper to plant root cells and possibly to fungal metalloenzymes that are strongly upregulated in symbiotic hyphae[47]. Indeed, upregulation of the *LbX325* gene was observed during the *Laccaria-Populus* ectomycorrhizal formation and also during fruiting body formation. These data draw a parallel with other work[48] showing that the knock out mutation of one of the *P. anserina*

X325 genes (XP_001907047.1, termed *IDC2*) led to the "Impaired for the Development of Crippled Growth" phenotype, an epigenetic cell degeneration associated with slow and abnormal growth as well as with sterility. In the endophytic fungus *Epichloë festucae*, the *X325* gene *SymB* (GenBank ID KX827271.1, sharing 75% identity with *IDC2*) is required for hyphal cell-cell fusion and maintenance of a mutualistic interaction with ray-grass (*Lolium perenne*)[49]. The X325 family also includes Bim1 from the pathogenic fungus *Cryptococcus neoformans*, where it is a critical factor in Cu acquisition in fungal meningitis[50]. Altogether, these data suggest that *in vivo*, X325 proteins may have an important role related to the morphogenesis and the development of the fungus and symbiosis with plants, for fungi for which this is a relevant part of the life-cycle.

Therefore, *Cn*BIM1, IDC2 and SymB and other members of the X325 family studied herein seem to hold biological functions in which copper is central. The interplay between X325 proteins and copper remains to be further investigated to understand the biological role of X325 proteins in filamentous fungi of different lifestyles.

Acknowledgements

A. Labourel was funded by a Marie Curie Individual Fellowship within the Horizon 2020 Research and Innovation Framework Programme (748758). The Danish Ministry of Higher Education and Science through the Instrument Center DANSCATT funded travel to synchrotrons. We also would like to acknowledge MAX-IV, Lund, Sweden, the ESRF, Grenoble, France and DESY, Hamburg, Germany, for synchrotron beamtime and related assistance. J-C. Poulsen is thanked for technical assistance and A. Kohler and D. Thiele for helpful discussions. F. Chaspoul is thanked for ICP-MS analyses and R. Balestrini (Institute for Sustainable Plant Protection, Italy) for providing gold-labeled wheat germ agglutinin

lectin. L. Lo Leggio and T. Tandrup thank the Novo Nordisk Foundation for funding through grant NF17SA0027704. K.E.H. Frandsen thanks the Carlsberg Foundation through an Internationalisation Postdoc Fellowship (grant n°CF16-0673 and n°CF17-0533) and the EU, framework of the Marie-Curie FP7 COFUND People Programme (AgreenSkills+ fellowship 609398) for financial support. L. Lo Leggio, T. Tandrup and K.E.H. Frandsen are members of ISBUC Integrative Structural Biology at the University of Copenhagen (www.isbuc.ku.dk). K.S. Johansen thanks the Novo Nordisk Foundation for funding through grant NNF17SA0027704. P.H. Walton and L. Ciano thank the UK Biotechnology and Biological Sciences Research Council (BB/L021633/1) for funding. F. Martin is funded by the French National Research Agency through the Laboratory of Excellence Advanced Research on the Biology of Tree and Forest Ecosystems (grant no. ANR-11-LABX 0002 01). A. Zerva thanks the French Embassy in Greece, together with the French Ministry of higher education, research and innovation, for the scholarship "Séjour scientifique de haut niveau" (SSHN). The electron microscopy experiments were performed on the PiCSL-FBI core facility (IBDM, Marseille), member of the France-BioImaging national research infrastructure (ANR-10-INBS-04).

Author contributions

A.L., D.N. and M.N.R. identified the new proteins. A.L. and B.H. performed bioinformatic analyses. A.L., S.G. and M.H. performed recombinant protein production and purification. T.T. and K.E.H.F. crystallized *La*X325, determined and analyzed the X-ray crystal structure; T.T. collected X-ray data; K.E.H.F. made relevant figures and tables; L.L.L. directed the crystallographic studies, K.E.H.F., K.S.J. and L.L.L. analyzed the structure and K.E.H.F. and L.L.L. drafted relevant parts of the manuscript. A.L., B.B. and A.Z. performed enzyme assays. M.F. and D.R. performed mass spectrometry analyses. L.C. and P.H.W. conceived and carried out the EPR study. A.L. and F.Z. performed confocal microscopy under the

supervision of F.M. A.L. and N.B. performed transmission electron microscopy. J.G.B. coordinated the work. A.L. and J.G.B. organized the data and drafted the manuscript. All authors made comments on the manuscript and approved the final version.

Competing Interests Statement

The authors declare no competing interests.

References

1. Vaaje-Kolstad, G. et al. An oxidative enzyme boosting the enzymatic conversion of recalcitrant polysaccharides. *Science* **330**, 219-222 (2010).

2. Quinlan, R.J. et al. Insights into the oxidative degradation of cellulose by a copper metalloenzyme that exploits biomass components. *Proc. Natl. Acad. Sci. U. S. A.* **108**, 15079-15084 (2011).

3. Horn, S.J., Vaaje-Kolstad, G., Westereng, B. & Eijsink, V.G. Novel enzymes for the degradation of cellulose. *Biotechnol. Biofuels* **5**, 45 (2012).

4. Bissaro, B. et al. Oxidative cleavage of polysaccharides by monocopper enzymes depends on H2O2. *Nat. Chem. Biol.* **13**, 1123 (2017).

5. Johansen, K. S. Discovery and industrial applications of lytic polysaccharide mono-oxygenases. *Biochem. Soc. Trans.* **44**, 143-149 (2016).

6. Bennati-Granier, C. et al. Substrate specificity and regioselectivity of fungal AA9 lytic polysaccharide monooxygenases secreted by *Podospora anserina*. *Biotechnol. Biofuels* **8**, 90 (2015).

7. Petrović, D.M. et al. Methylation of the N-terminal histidine protects a lytic polysaccharide monooxygenase from auto-oxidative inactivation. *Protein Sci.* **27**, 1636-1650 (2018).

8. Ciano, L., Davies, G.J., Tolman, W.B. & Walton, P.H. Bracing copper for the catalytic oxidation of C–H bonds. *Nat. Catal.* **1**, 571-577 (2018).

9. Gilbert, H.J., Knox, J.P. & Boraston, A.B. Advances in understanding the molecular basis of plant cell wall polysaccharide recognition by carbohydrate-binding modules. *Curr. Opin. Struc. Biol.* **23**, 669-677 (2013).

10. Hemsworth, G.R., Henrissat, B., Davies, G.J. & Walton, P.H. Discovery and characterization of a new family of lytic polysaccharide monooxygenases. *Nat. Chem. Biol.* **10**, 122-126 (2014).

11. Lo Leggio, L. et al. Structure and boosting activity of a starch-degrading lytic polysaccharide monooxygenase. *Nat. Commun.* **6**, 5961 (2015).

12. Vu, V.V., Beeson, W.T., Span, E.A., Farquhar, E.R. & Marletta, M.A. A family of starch-active polysaccharide monooxygenases. *Proc. Natl. Acad. Sci. U. S. A.* **111**, 13822-13827 (2014).

13. Sabbadin, F. et al. An ancient family of lytic polysaccharide monooxygenases with roles in arthropod development and biomass digestion. *Nat. Commun.* **9**, 756 (2018).

14. Couturier, M. et al. Lytic xylan oxidases from wood-decay fungi unlock biomass degradation. *Nat. Chem. Biol.* **14**, 306 (2018).

15. Filiatrault-Chastel, C. et al. AA16, a new lytic polysaccharide monooxygenase family identified in fungal secretomes. *Biotech. for Biofuels* **12**, 55 (2019).

16. Berrin, J.-G., Rosso, M.-N. & Abou Hachem, M. Fungal secretomics to probe the biological functions of lytic polysaccharide monooxygenases. *Carbohydr. Res.* **448**, 155-160 (2017).

17. Navarro, D. et al. Fast solubilization of recalcitrant cellulosic biomass by the basidiomycete fungus *Laetisaria arvalis* involves successive secretion of oxidative and hydrolytic enzymes. *Biotechnol. Biofuels* **7**, 143 (2014).

18. Kelley, L.A., Mezulis, S., Yates, C.M., Wass, M.N. & Sternberg, M.J.E. The Phyre2 web portal for protein modeling, prediction and analysis. *Nat. Protocols* **10**, 845-858 (2015).

19. Forsberg, Z. et al. Structural and functional characterization of a conserved pair of bacterial cellulose-oxidizing lytic polysaccharide monooxygenases. *Proc. Natl. Acad. Sci. U. S. A.* **111**, 8446-8451 (2014).

20. Low, M. & Saltiel, A. Structural and functional roles of glycosyl-phosphatidylinositol in membranes. *Science* **239**, 268-275 (1988).

21. Berbee, M.L., James, T.Y. & Strullu-Derrien, C. Early diverging fungi: diversity and impact at the dawn of terrestrial life. *Annu. Rev. Microbiol.* **71**, 41-60 (2017).

22. Tandrup, T., Frandsen, K.E.H., Johansen, K.S., Berrin, J.-G. & Lo Leggio, L. Recent insights into lytic polysaccharide monooxygenases (LPMOs). *Biochem. Soc. Trans.* **46**, 1431-1447 (2018).

23. Holm, L. & Laakso, L.M. Dali server update. *Nucleic Acids Res.* **44**, W351-W355 (2016).

24. Vu, V.V. & Ngo, S.T. Copper active site in polysaccharide monooxygenases. *Coordination Chem. Rev.* **368**, 134-157 (2018).

25. Chiu, E. et al. Structural basis for the enhancement of virulence by viral spindles and their in vivo crystallization. *Proc. Natl. Acad. Sci. U. S. A.* **112**, 3973-3978 (2015).

26. Tan, T.-C. et al. Structural basis for cellobiose dehydrogenase action during oxidative cellulose degradation. *Nat. Commun.* **6**, 7542 (2015).

27. Lawton, T.J., Kenney, G.E., Hurley, J.D. & Rosenzweig, A.C. The CopC family: structural and bioinformatic insights into a diverse group of periplasmic copper binding proteins. *Biochemistry* **55**, 2278-2290 (2016).

28 Ross, M.O. et al. Particulate methane monooxygenase contains only mononuclear copper centers. *Science* **364**, 566-570 (2019).

29 Liew, E.F., Tong, D., Coleman, N.V. & Holmes, A.J. Mutagenesis of the hydrocarbon monooxygenase indicates a metal centre in subunit-C, and not subunit-B, is essential for copper-containing membrane monooxygenase activity. *Microbiology* **160**, 1267-1277 (2014).

30. Cao, L., Caldararu, O., Rosenzweig, A.C. & Ryde, U. Quantum refinement does not support dinuclear copper sites in crystal structures of particulate methane monooxygenase. *Angew. Chem. Int. Ed.* **57**, 162-166 (2018).

31. Peisach, J. & Blumberg, W.E. Structural implications derived from the analysis of electron paramagnetic resonance spectra of natural and artificial copper proteins. *Arch. Biochem. Biophys.* **165**, 691-708 (1974).

459 32. Kuusk, S. et al. Kinetics of H_2O_2-driven degradation of chitin by a bacterial lytic
460 polysaccharide monooxygenase. *J. Biol. Chem.* **293**, 523-531 (2018).

461 33. Hangasky, J.A., Iavarone, A.T. & Marletta, M.A. Reactivity of O_2 versus H_2O_2 with
462 polysaccharide monooxygenases. *Proc. Natl. Acad. Sci. U. S. A.* **115**, 4915-4920 (2018).

463 34. Phillips, C.M., Beeson, W.T., Cate, J.H. & Marletta, M.A. Cellobiose dehydrogenase and a
464 copper-dependent polysaccharide monooxygenase potentiate cellulose degradation by *Neurospora*
465 *crassa*. *ACS Chem. Biol.* **6**, 1399-1406 (2011).

466 35. Bey, M. et al. Cello-oligosaccharide oxidation reveals differences between two lytic
467 polysaccharide monooxygenases (family GH61) from *Podospora anserina*. *Appl. Environ. Microbiol.*
468 **79**, 488-496 (2013).

469 36. Chen, K.H. et al. Bacteriohemerythrin bolsters the activity of the particulate methane
470 monooxygenase (pMMO) in *Methylococcus capsulatus* (Bath). *J. Inorg. Biochem.* **111**, 10-17 (2012).

471 37. Bernardes et al. Carbohydrate binding modules enhance cellulose enzymatic hydrolysis by
472 increasing access of cellulases to the substrate. *Carbohydr. Polym.* **211**, 57-68 (2019).

473 38. Shah, F. et al. Ectomycorrhizal fungi decompose soil organic matter using oxidative
474 mechanisms adapted from saprotrophic ancestors. *New Phytol.* **209**, 1705-1719 (2016).

475 39. Balestrini R. M.& Kottke I. Structure and development of ectomycorrhizal roots. in *Molecular*
476 *Mycorrhizal Symbiosis* (ed. Martin, F.) 47-62 (John Wiley & Sons, Hoboken, New Jersey, 2016).

477 40. Balestrini, R., Hahn, M.G., Faccio, A., Mendgen, K. & Bonfante, P. Differential localization
478 of carbohydrate epitopes in plant cell walls in the presence and absence of arbuscular mycorrhizal
479 fungi. *Plant Physiology* **111**, 203-213 (1996).

480 41. Balestrini, R. & Bonfante, P. Cell wall remodeling in mycorrhizal symbiosis: a way towards
481 biotrophism. *Front. Plant Sci*. **5**, 237 (2014).

42. Yamazaki, H., Tanaka, A., Kaneko, J.-i., Ohta, A. & Horiuchi, H. *Aspergillus nidulans* ChiA is a glycosylphosphatidylinositol (GPI)-anchored chitinase specifically localized at polarized growth sites. *Fungal Genet. Biol.* **45**, 963-972 (2008).

43. Nakajima, M., Yamashita, T., Takahashi, M., Nakano, Y. & Takeda, T. A novel glycosylphosphatidylinositol-anchored glycoside hydrolase from *Ustilago esculenta* functions in β-1,3-glucan degradation. *Appl. Environ. Microbiol.* **78**, 5682-5689 (2012).

44. Smith, H.W. & Marshall, C.J. Regulation of cell signalling by uPAR. *Nat. Rev. Mol. Cell Biol.* **11**, 23 (2010).

45. Gaggelli, E., Kozlowski, H., Valensin, D. & Valensin, G. Copper homeostasis and neurodegenerative disorders (Alzheimer's, prion, and Parkinson's diseases and amyotrophic lateral sclerosis). *Chem. Rev.* **106**, 1995-2044 (2006).

46. García-Santamarina, S. & Thiele, D.J. Copper at the fungal pathogen-host axis. *J. Biol. Chem.* **290**, 18945-18953 (2015).

47. Bolchi, A. et al. Genome-wide inventory of metal homeostasis-related gene products including a functional phytochelatin synthase in the hypogeous mycorrhizal fungus *Tuber melanosporum*. *Fungal Genet. Biol.* **48**, 573-584 (2011).

48. Lalucque, H. et al. IDC2 and IDC3, two genes involved in cell non-autonomous signaling of fruiting body development in the model fungus *Podospora anserina*. *Dev. Biol.* **421**, 126-138 (2017).

49. Green, K.A. et al. SymB and SymC, two membrane associated proteins, are required for *Epichloë festucae* hyphal cell–cell fusion and maintenance of a mutualistic interaction with *Lolium perenne*. *Mol. Microbiol.* **103**, 657-677 (2016).

50. García-Santamarina, S. et al. A Lytic Polysaccharide Monooxygenase-like protein functions in copper import and fungal meningitis. *Nat. Chem. Biol*. In press.

Figure legends

Figure 1: Phylogeny of the X325 family.

The phylogenetic tree was built with 123 protein sequences originating from 58 different genomes. Green patches highlight the clades. Nodes with a red oval shape show the X325s selected and characterized in this study. The diamond node shows the *Cryptococcus neoformans* X325 (*Cn*BIM1). Light blue nodes with the star shape highlight the sequences displaying a histidine instead of the aspartate residue in the active site. The asterisk indicates the sequence belonging to early-diverging Mucoromycotina (not part of basidiomycetes). Modularity and sequence alignment of family X325 are presented in **Supplementary Figure 1**.

Figure 2: Structure of X325 and configuration of the copper active site.

(**a**) Overall three-dimensional structure of *La*X325 (grey) and active site residues (cyan). (**b**) From top to bottom: Active sites (histidine brace) of *La*X325 (cyan) and *Td*AA15 (green), and the copper binding site of CopC (magenta) and the Cu_B center of *Methylocystis* pMMO (yellow) aligned with respect to the N-terminal His. Equatorial Cu-coordination is indicated with full lines. In *La*X325 the copper atom is coordinated by His1, His49, Asp122 and a water molecule in the axial position (red sphere). (**c**) Continuous wave X-band EPR spectrum with simulation (red) of *La*X325. More data are presented in **Supplementary Figures 2, 3** and **4**.

Figure 3: *La*X325 structural and biochemical features do not support LPMO-type activity.

(a) Superimposition of *La*X325 and *Ls*AA9A in complex with its polysaccharide substrate (aligned with respect of the N-terminal His). The *La*X325 structure (green, PDB 6IBJ) is shown in cartoon with His1 and Asp122 shown in sticks. The GGDG loop is shown in red and

the C-terminus shown in magenta (sphere represents the first His of the $(His)_6$-tag that substitutes the GPI anchor in the recombinant protein). The surface of *Ls*AA9A (PDB 5ACI) is shown in grey and the structure is shown in ribbon (black). His1, Tyr203 and cellohexaose of *Ls*AA9A are shown in cyan sticks. (**b**) The action of X325 proteins on cellulose (Avicel) was investigated and compared to *Pa*LPMO9E, a C1 cellulose-acting AA9 LPMO. Assays were performed in the presence of L-cysteine (1 mM). In the control condition, X325 protein was replaced by $CuSO_4$ at the same concentration (1 µM). Samples were analyzed by ionic chromatography. Cellohexaose (DP_6) is eluted at the same retention time as cellobionic acid (DP_{2ox}). The experiments were repeated three times independently. More data supporting the absence of LPMO-type activity of X325 proteins are presented in **Supplementary Figure 5**.

Figure 4: Immunolocalization of *Lb*X325 in *Laccaria bicolor*.

(**a**) Bright field observation of transverse sections of 3-weeks-old ectomycorrhiza. (**b**) Transverse sections of 3-weeks-old ectomycorrhiza stained for *Lb*X325 with anti-*Lb*X325 immune serum (green) and for chitin with WGA (red). Images **a** and **b** were obtained by using indirect immunofluorescence confocal laser microscopy. **c**, Transmission electron micrograph obtained after post-embedding double-immunogold labelling of ultra-thin transverse sections of 3-weeks-old ectomycorrhiza. **d**, Zoomed-in view of **c**. Chitin is identified with wheat germ agglutinin (WGA) coupled to 15 nm gold particles (highlighted by red arrows). *Lb*X325 is identified with a secondary antibody coupled to 6 nm gold particles (highlighted by blue arrows). RC = root cell, FC = fungal cell. Selected images are representative of five different sections. More data are presented in **Supplementary Figures 6, 7** and **8**.

On-line Materials and Methods

Transcriptomics and secretomics data

Transcriptomic and proteomic data of cultures of *Laetisaria arvalis* strain BRFM514 grown on cellulose (Avicel), wheat straw, wheat straw residue following traditional saccharification and maize bran are described in [17]. Transcriptomic data of *Laccaria bicolor* strain S238N are described in [51].

Bioinformatic analysis of X325

L. arvalis X325 sequence (Genbank ID MK088083) was compared to the NCBI non redundant sequence database using BlastP[55] in December 2017. Blast searches conducted with X325 did not retrieve AA9s, AA10s, AA11s, AA13s, AA14s or AA15s with significant scores. MUSCLE[56] was used to perform multiple alignments. To avoid interference from the presence or absence of additional residues, the signal peptides and C-terminal extensions (linker and GPI anchor) were removed. Bioinformatic analyses were performed on 58 fungal genomes sequenced and shared by JGI collaborators. A phylogenetic tree has been inferred using 123 cleaned and merged alignments of proteins from selected clusters of proteins. Those clusters are present, as much as possible, in all fungi in one copy in order to maximize the score $\sum 1/n$ (with n, the number of copy in the genome). Sequences from clusters were aligned with MUSCLE and a phylogenetic tree was built using BOOSTER[57] (https://booster.pasteur.fr/) with 200 Bootstrap replicates and Fasttree as workflow. The tree is displayed with Dendroscope[58].

Production of X325 proteins

The sequences corresponding to *LaX325* (Genbank ID MK088083), *LbX325* (Genbank ID XM_001874260.1), *PaX325* (Genbank ID XM_001907524.1) and *YlX325* (Genbank ID XM_505821.1) genes were synthesized after codon optimization for expression in *P. pastoris*

(GenScript, Piscataway, USA). The region corresponding to the native signal sequence was kept while the C-terminal GPI anchor was removed. Synthesized genes were further inserted into a modified pPICZαA vector (Invitrogen, Cergy-Pontoise, France) using *Bst*BI and *Xba*I restriction sites in frame with the $(His)_6$-tag located at the C-terminus of recombinant proteins. Site-directed mutagenesis of the Asp116 residue of *Yl*X325 to either a Ser or His residue was performed using the Quikchange site-directed mutagenesis kit (Agilent, Les Ulis, France) following manufacturer's conditions. Transformation of competent *P. pastoris* X33 was performed by electroporation with PmeI-linearized pPICZαA recombinant plasmids and zeocin-resistant *P. pastoris* transformants were screened for protein production as described in [59]. The best-producing transformants were grown in 2 L of BMGY medium in shaken flasks at 30°C in an orbital shaker (200 rpm) to an OD_{600} of 2 to 6. Cells were then transferred to 400 mL of BMMY medium containing 1 $mL.L^{-1}$ of PTM_4 salts at 20°C in an orbital shaker (200 rpm) for 3 days, with supplementation of 3% (v/v) methanol every day. *P. pastoris* strain X33 and the pPICZαA vector are components of the *P. pastoris* Easy Select Expression System (Invitrogen), all media and protocols are described in the manufacturer's manual (Invitrogen).

Purification of X325 proteins

The culture supernatants were recovered by pelleting the cells by centrifugation at 2,700 *g* for 5 min, 4°C and filtered on 0.45 µm filters (Millipore, Molsheim, France). For $(His)_6$-tagged enzymes, the pH was adjusted to 7.8 and the supernatants were loaded onto 5 mL His Trap HP columns (GE healthcare, Buc, France) connected to an Akta Xpress system (GE healthcare). Prior to loading, the columns were equilibrated in 50 mM Tris HCl pH 7.8; 150 mM NaCl (buffer A). The loaded columns were then washed with 5 column volumes (CV) of 10 mM imidazole in buffer A, before the elution step with 5 CV of 150 mM imidazole in buffer A. Fractions containing the protein were pooled and concentrated with a 3-kDa

vivaspin concentrator (Sartorius, Palaiseau, France) and buffer exchanged in 50 mM sodium acetate buffer pH 5.2. The concentrated proteins were then incubated with ten-fold molar equivalent of $CuSO_4$ overnight in cold room and buffer exchange in 50 mM sodium acetate buffer pH 5.2 to remove $CuSO_4$ excess.

Biochemical analysis of X325s

Concentration of purified proteins was determined by using a nanodrop ND-2000 device with calculated molecular mass and molar extinction coefficients derived from the sequences. Proteins were loaded onto 10% SDS-PAGE gels (Thermo Fisher Scientific, IL, USA), which were stained with Coomassie Blue. The molecular mass under denaturating conditions was determined with reference standard proteins (Page Ruler Prestained Protein Ladder, Thermo Fisher Scientific).

N-terminal amino acid sequence determination

The N-terminal amino acid sequence of purified *La*X325 was determined according to the Edman degradation. Samples were electroblotted onto a polyvinylidene difluoride membrane (iBlot, Life Technologies). Analyses were carried out on a Procise Sequencing System (Thermofisher).

Tandem mass spectrometry analyses (MS/MS)

Experiments were performed on a Synapt G2Si high-definition mass spectrometer (Waters Corp., Manchester, UK) equipped with an Electrospray ion (ESI) source. Oxidized species were isolated and fragmented by collision-induced dissociation in the transfer cell of the instrument (MS/MS). In these experiments, ion mobility (IM) was activated to reduce interference from sample impurities. IM was performed in a traveling-wave ion mobility (TWIM) cell. Helium flows was held at 180 $mL.min^{-1}$ in the helium cell and nitrogen flow

623 was adjusted at 90 mL.min^{-1} in the mobility cell. The IM traveling wave height was set to 40
624 V, and its wave velocity was set to 300 m.s^{-1}. Samples were diluted ten-fold in MeOH/H_2O
625 (1:1, v/v) and infused at a flow rate of 5 µL.min^{-1}. Acquisitions were conducted in negative
626 polarity, as well as in 'sensitivity' mode.

627 **ICP/MS Analysis**

628 Prior to the analysis, samples were mineralized in a mixture containing 2/3 of nitric acid
629 (Sigma-Aldrich, 65% Purissime) and 1/3 of hydrochloric acid (Fluka, 37%, Trace Select) at
630 120°C. The residues were diluted in ultra-pure water (2 mL) before Inductively Coupled
631 Plasma/Mass Spectrometry (ICP/MS) analysis. The ICP-MS instrument was an ICAP Q
632 (ThermoElectron, Les Ullis, France), equipped with a collision cell. The calibration curve was
633 obtained by dilution of a certified multi-element solution (Sigma-Aldrich). Copper
634 concentrations were determined using Plasmalab software (Thermo-Electron), at a mass of
635 interest *m/z* = 63.

636 **Polysaccharides cleavage assays**

637 Avicel was purchased from Sigma-Aldrich and lichenan (from Icelandic moss), xylan,
638 tamarind xyloglucan, barley β-1,3/1,4-glucan, konjac glucomannan, wheat arabinoxylan,
639 pachyman, pustulan, chitin and chitosan were purchased from Megazyme (Wicklow, Ireland).
640 The *L. bicolor* cell wall extract was supplied by Feng Zhang (INRA, Nancy, France).

641 All the cleavage assays contained 1 µM of enzyme or 1 µM $CuSO_4$ in the presence of 1 mM
642 L-cysteine, 0.5% (w/v) polysaccharides and 50 mM sodium acetate buffer pH 5.2. Lignin
643 fractions extracted from softwood and duroquinol (Sigma Aldrich) were also tested as
644 reducing agent. The enzyme reactions were performed in 2-mL tubes and incubated in a
645 thermomixer (Eppendorf, Montesson, France) at 40°C and 850 rpm. After 16 h of incubation,
646 samples were heated for 10 min at 100°C to stop the enzymatic reaction and then centrifuged

at 14,000 *g* for 15 min at 4°C to separate the soluble fraction from the remaining insoluble fraction before determination of soluble products using HPAEC as described above with oligosaccharides standards (Megazyme).

Polysaccharides cleavage assays under anaerobic conditions

To assess the monooxygenase activity of X325 proteins, the different reagent solutions used to compose the reaction mixtures were made anaerobic separately. Solutions of water, buffer (200 mM sodium acetate pH 5.2), Avicel (1% (w/v)) and NaOH (2 M) were submitted to 10 min sonication followed by 10 min flushing with nitrogen gas before being placed in an anaerobic chamber (Jacomex GP Campus, Dagneux, France) for 48 hours to ensure complete O_2-free conditions (the lids of the vessels were slightly loose). The stock solution of copper-loaded protein and $CuSO_4$ were frozen in liquid nitrogen and let thawed in the anaerobic chamber to equilibrate with anaerobic atmosphere during 48 hours. L-cysteine was placed in the anaerobic chamber as a powder during 48 hours and dissolved in anaerobic water before the experiment.

To set-up reactions, the copper-loaded protein or $CuSO_4$ (5 µM final concentration) was added to anaerobic Avicel suspension (0.5% (w/v) final concentration) in 50 mM sodium acetate buffer pH 5.2. L- cysteine was added to all the reactions to a final concentration of 1 mM. 50 µM of H_2O_2 was added to the first third of the reactions, while water was added instead to the second and third third of the reactions to a final volume of 200 µL. While the second third was kept in the anaerobic chamber (i.e. anaerobic control) the third third was taken out of the anaerobic chamber and re-equilibrated with atmospheric O_2 by vigorous mixing. The aerobic reactions constitute positive controls ensuring that the treatment of the different stock solutions (enzyme, L-cysteine) did not harm the integrity of the reactants. After 16 hours incubation at 23°C, all reactions were stopped by addition of 10 µL NaOH solution

671 (0.1 M final). All samples were centrifuged before analysis of soluble products by HPAEC-
672 PAD as described above. Reactions were performed as triplicate independent experiments.

673 **Production of antibodies, protein electrophoresis and Western immunoblotting**

674 A solution of 5 mg of purified recombinant *Lb*X325 protein was used to elicit rabbit
675 polyclonal antibodies according to the manufacturer's procedure (Eurogentec, Seraing,
676 Belgium). Total proteins from free-living mycelium, 15 ectomycorrhizal roots were extracted
677 according to literature[60]. Protein analyses were carried out by using 4–20% Mini-Protean
678 TGX Precast Protein gels in a Mini-Protean electrophoresis cell system (both Bio-Rad).
679 Specificity of the antibodies was determined by western blot of total protein obtained from
680 poplar lateral roots not in contact with *L. bicolor* S238N and from mycorrhizal root tips using
681 the Bio-Rad alkaline phosphatase immune-blot kit (Bio-Rad Laboratories) according to the
682 manufacturer's instructions.

683 **Confocal microscopy and indirect immunofluorescence localization**

684 Three-week-old ectomycorrhizal root tips from grey poplar (cv INRA 717-1-B4) or free
685 living mycelium of *L. bicolor* S238N were fixed for 4 h in 4% (w/v) paraformaldehyde in
686 phosphate-buffered saline (PBS) (137 mM NaCl, 2.7 mM KCl, 10 mM Na_2HPO_4, 1.8 mM
687 K_2HPO_4, pH 7.4). The root segments were embedded in agarose 4% (w/v) and cut into 25 µm
688 longitudinal or 25–30 µm radial sections with a Leica VT1200S Leica vibratome (Leica
689 Microsystems, Nanterre, France). Sections were retrieved with a brush and carefully
690 transferred onto watch glasses and then were stained according to literature[61]. The indirect
691 immunofluorescent localization of the *Lb*X325 protein was performed by confocal
692 microscopy as described by[62].

693

Transmission electron microscopy

Three-week-old ectomycorrhizal root tips from grey poplar (cv INRA 717-1-B4) or free-living mycelium (FLM) of *L. bicolor* S238N were dissected from the agar plate and fixed with 2.5% glutaraldehyde, 2% paraformaldehyde in PBS for 2 h. The samples were washed in PBS and embedded in 4% agarose. Vibratome sections of 80 µm thickness were made and post-fixed in 1% osmium tetroxide in distilled water for 1h, washed and incubated in uranyl acetate 1% in distilled water overnight at 4°C. Vibratome sections were dehydrated in ethanol and acetone, and embedded in epon resin. Ultrathin 70 nm-sections were performed on a UC7 Leica Ultramicrotome (Leica, Netherlands).

Sections on nickel grids were incubated with saturated sodium metaperiodate for 2 min. The grids were washed rapidly in TBS with 1% Triton X-100. The grids were then incubated with 10 % normal serum in TBS for 1 hour, followed by an overnight incubation with rabbit anti-*Lb*X325 antibodies (1/20) at 4°C. The grids were washed in TBS and incubated with secondary antibodies (6 nm anti-rabbit, Aurion, 1/15) for 1 hour, then washed again in TBS. The grids were incubated for 10 min in 2.5 % glutaraldehyde in 0.05 M cacodylate buffer, washed, and free aldehydes groups were quenched (0.1 M glycine in TBS for 10 min). The grids were then stained with WGA-15nm conjugate for 40 min, washed in water and counter-stained by 1% uranyl acetate (5 min) and lead citrate (2 min). Acquisitions were performed on a Tecnai G2 at 200 kV (FEI, Netherlands). Micrographs were acquired with a Veleta camera (Olympus, Japan).

Structure determination by X-ray crystallography

To remove N-linked glycans, 20 mg of purified enzymes were treated with 500,000 U of EndoH (New England Biolabs, Ipswich, MA) under native conditions (48 h at 20°C) according to the manufacturer's instructions. Deglycosylated and control samples were

analyzed by SDS-PAGE (**Supplementary Figure 9**). To remove EndoH, buffer A was added to the sample and purification was performed using a 5 mL His Trap HP columns (GE healthcare, Buc, France) connected to an Akta Xpress system (GE healthcare) as described above. Fractions containing the protein were pooled and concentrated with a 3-kDa vivaspin concentrator (Sartorius, Palaiseau, France) and buffer exchanged in 20 mM MES buffer pH 6.0.

Crystals were grown using the sitting-drop vapor diffusion technique set up in MRC plates (Molecular dimensions) with 100 µL reservoirs at room temperature, using an Oryx-8 robot (Douglas Instruments). *La*X325 (13.3 $mg.mL^{-1}$ in 20 mM MES pH 6.0) was incubated with copper acetate in a 1:1 molar ratio for 1 hour at 4°C. Addition of copper acetate made the sample precipitate, however, the precipitate dissolved again after 1 hour incubation. Screening was carried out using the commercial JCSG+ and Morpheus screens (Molecular Dimensions). Crystals were harvested and flash frozen in liquid nitrogen without added cryoprotectant. Two initial datasets were collected at a wavelength of 0.9799 Å at the BioMAX beamline of MAXIV on *La*X325 crystals grown from Morpheus conditions #40 ($P2_1$ dataset in **Supplementary Table 2**) and #85 ($P4_32_12$ dataset in **Supplementary Table 2**) in a volume ratio of 1:1 (enzyme:reservoir solution) and 13.3 mg/mL *La*X325 in the protein stock solution. Morpheus screen #40 has the following composition: 20 mM 1,6-hexanediol, 20 mM 1-butanol, 20 mM (RS)1,2-propandiol, 20 mM 2-propanol, 20 mM 1,4-butandiol, 2 mM 1,3-propandiol, 100 mM MES monohydrate pH 6.5, 100 mM imidazole pH 6.5, 12.5% (w/v) MPD, 12.5% (w/v) PEG1000, 12.5% (w/v) PEG3350. Morpheus screen #85 has the following composition: 20 mM L-Na-Glutamate, 20 mM DL-Alanine (racemic), 20 mM Glycine, 20 mM DL-Lysine HCl (racemic), 20 mM DL-Serine (racemic), 100 mM MES monohydrate pH 6.5, 100 mM imidazole pH 6.5, 20% (w/v) PEG 500 MME and 10% (w/v) PEG 20,000. The structure could not be determined from these datasets due to limited anomalous signal at the

743 data collection wavelength. The original crystals could not be reproduced spontaneously, but
744 required seeding, either using the Oryx-8 robot, or by streak seeding using a horse hair. A
745 third dataset (in $P2_12_12_1$, **Supplementary Table 2**) was collected from a crystal of *La*X325
746 grown by streak seeding into the Morpheus[63] #85 condition. Data was collected at beamline
747 ID29 at the ESRF, using a wavelength of 1.299 Å, close to the copper edge, with an
748 oscillation of 0.1° and 4000 images for high redundancy. The structure was solved using
749 anomalous dispersion methods, by running Phenix.autosol[64] searching for 4-6 sites (as
750 indicated by the Matthew's coefficient) using data automatically processed and scaled to 2.08
751 Å resolution in $P2_12_12_1$ with XDS and XSCALE[65]. Two additional structures in different
752 space groups were determined by Molecular Replacement with MOLREP[66] and refined with
753 Refmac5[67] (of the CCP4 suite) using this initial structure (in $P2_12_12_1$) as search model and the
754 previously collected $P4_32_12$ and $P2_1$ datasets scaled to 2.10 Å and 1.82 Å resolution,
755 respectively. For all structures 100% of the residues were in the allowed regions of the
756 Ramachandran plot. Crystals of *La*X325 grown from seeds in both Morpheus condition #40
757 and #85 were soaked for 50-60 minutes in 5 mM L-Cysteine (Sigma Aldrich) dissolved in
758 reservoir conditions. Diffraction data could be collected to close to 2 Å resolution at the P11
759 beam line of Petra-III, DESY, Hamburg, Germany, but only on orthorhombic crystals. No
760 dataset collected resulted in any conformational changes of amino acids as a function of the
761 reduction of the Cu-atom. The max dose experienced by the crystals were estimated to 724.78
762 KGy using RADDOSE-3D[68]. All datasets were collected at cryogenic temperatures (100 K).
763 Crystallization attempts of *Lb*X325 were not successful.

764

765 **Electron Paramagnetic Resonance (EPR) spectroscopy**

766 Continuous wave (cw) X-band frozen solution EPR spectra of a 0.2 mM solution of Cu(II)-
767 *La*X325 in 50 mM sodium acetate buffer pH 5.2 were recorded on a Bruker EMX

768 spectrometer operating at ~9.30 GHz, with modulation amplitude of 4 G, modulation
769 frequency of 100 kHz and microwave power of 10.02 mW at 165 K. To check possible
770 binding of copper to the His-tag, a copper titration was performed starting from the apo-
771 enzyme and adding 0.2 equivalents of Cu (from a $CuCl_2$ stock in water) in 2 µL injections,
772 which showed binding exclusively to the LPMO active site until addition of ca. one
773 equivalent of Cu (**Supplementary Figure 3**). Addition of Avicel to the EPR sample did not
774 cause any change to the spectrum of *La*X325.

775 Spectral simulations were carried out using EasySpin[69] 5.2.16 integrated in MatLab software.
776 Simulation parameters are given in **Supplementary Table 4**. It was assumed that g and A
777 tensors were axially coincident. g_z and $|A_z|$ values were determined accurately from the
778 absorption at low field. Accurate determination of the g_x, g_y, $|A_x|$ and $|A_y|$ values was not
779 possible due to the second order nature of the perpendicular region, although it was noted that
780 satisfactory simulation could only be achieved with the particular set of values reported in
781 **Supplementary Table 4**. Furthermore, it was noted that the simulations were improved by
782 the addition of coupled nitrogen atoms, although the exact value of the coupling could not be
783 determined given the lack of well resolved superhyperfine coupling. Raw EPR data are
784 available on request through the Research Data York (DOI: 10.15124/a034974e-2782-415e-
785 8b02-2b6e4098760e).

786

787 **Data availability statement**

788 *La*X325 nucleotide sequence was deposited in GenBank under accession number MK088083.
789 The X-ray structures of *La*X325 were deposited in the Protein Data Bank with accession
790 numbers 6IBH, 6IBI, 6IBJ. Raw EPR data are available on request through the Research Data
791 York (10.15124/a034974e-2782-415e-8b02-2b6e4098760e).

Methods-only references

54. Kohler, A. et al. Convergent losses of decay mechanisms and rapid turnover of symbiosis genes in mycorrhizal mutualists. *Nat. Genet.* **47**, 410 (2015).

55. Altschul, S.F., Gish, W., Miller, W., Myers, E.W. & Lipman, D.J. Basic local alignment search tool. *J. Mol. Biol.* **215**, 403-410 (1990).

56. Edgar, R.C. MUSCLE: multiple sequence alignment with high accuracy and high throughput. *Nucleic Acids Res.* **32**, 1792-1797 (2004).

57. Lemoine, F. et al. Renewing Felsenstein's phylogenetic bootstrap in the era of big data. *Nature* **556**, 452-456 (2018).

58. Huson, D.H. & Scornavacca, C. Dendroscope 3: an interactive tool for rooted phylogenetic trees and networks. *Syst. Biol.* **61**, 1061-1067 (2012).

59. Haon, M. et al. Recombinant protein production facility for fungal biomass-degrading enzymes using the yeast *Pichia pastoris*. *Front. Microbiol.* **6**, 1002-1002 (2015).

60. Pitarch, A., Sánchez, M., Nombela, C. & Gil, C. Sequential fractionation and two-dimensional gel analysis unravels the complexity of the dimorphic fungus *Candida* albicans cell wall proteome. *Mol. Cell. Proteomics* **1**, 967-982 (2002).

61. Felten, J. et al. The ectomycorrhizal fungus *Laccaria bicolor* stimulates lateral root formation in poplar and *Arabidopsis* through auxin transport and signaling. *Plant Physiol.* **151**, 1991-2005 (2009).

62. Martin, F. et al. The genome of *Laccaria bicolor* provides insights into mycorrhizal symbiosis. *Nature* **452**, 88 (2008).

63. Gorrec, F. The MORPHEUS protein crystallization screen. *J. Appl.Crystallogr.* **42**, 1035-1042 (2009).

64. Terwilliger, T.C. et al. Decision-making in structure solution using Bayesian estimates of map quality: the PHENIX AutoSol wizard. *Acta Cryst. D* **65**, 582-601 (2009).

65. Kabsch, W. XDS. *Acta Cryst.* **66**, 125-132 (2010).

66. Vagin, A. & Teplyakov, A. Molecular replacement with MOLREP. *Acta Cryst.D* **66**, 22-25 (2010).

67. Murshudov, G.N. et al. REFMAC5 for the refinement of macromolecular crystal structures. *Acta Cryst.D* **67**, 355-367 (2011).

68. Zeldin, O.B., Gerstel, M. & Garman, E.F. RADDOSE-3D: time- and space-resolved modelling of dose in macromolecular crystallography. *J. Appl. Crystallogr.* **46**, 1225-1230 (2013).

69. Stoll, S. & Schweiger, A. EasySpin, a comprehensive software package for spectral simulation and analysis in EPR. *J. Mag. Res.* **178**, 42-55 (2006).

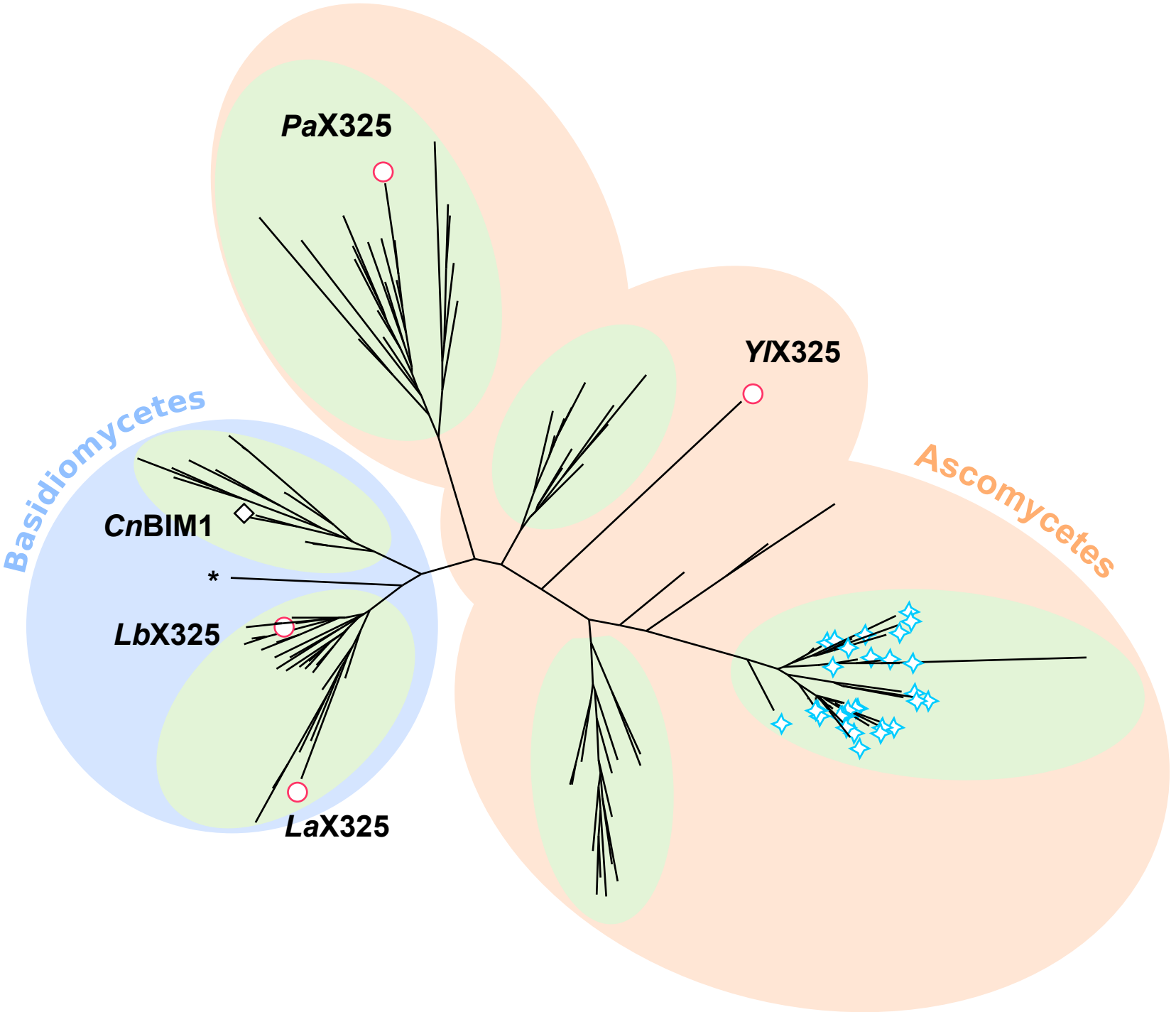
PaX325
YlX325
Basidiomycetes
Ascomycetes
CnBIM1
*
LbX325
LaX325

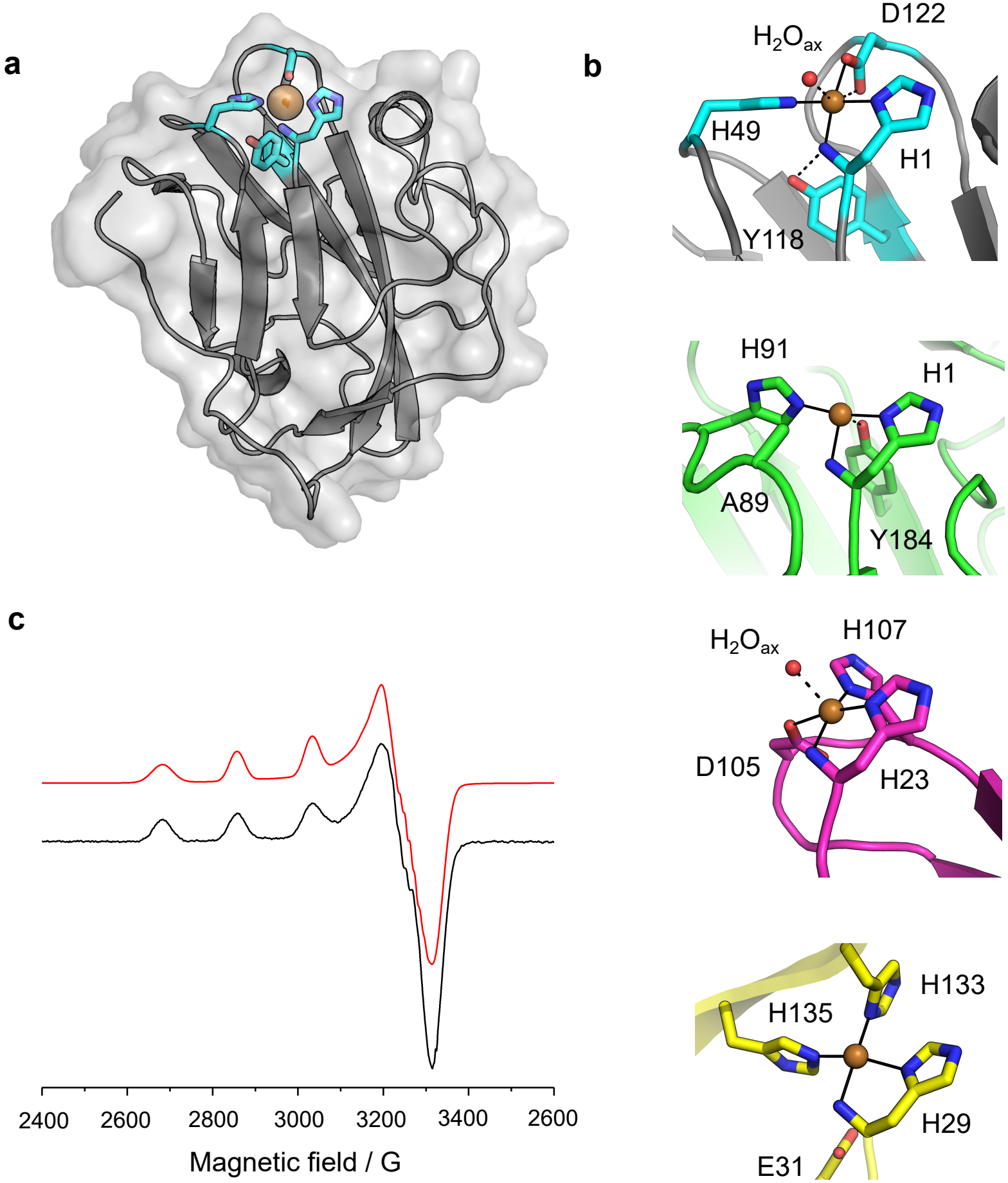
a
b
D122
H_2O_{ax}
H49
H1
Y118
H91
H1
A89
Y184
c
H_2O_{ax}
H107
D105
H23
H133
H135
H29
E31
2400
2600
2800
3000
3200
3400
2600
Magnetic field / G

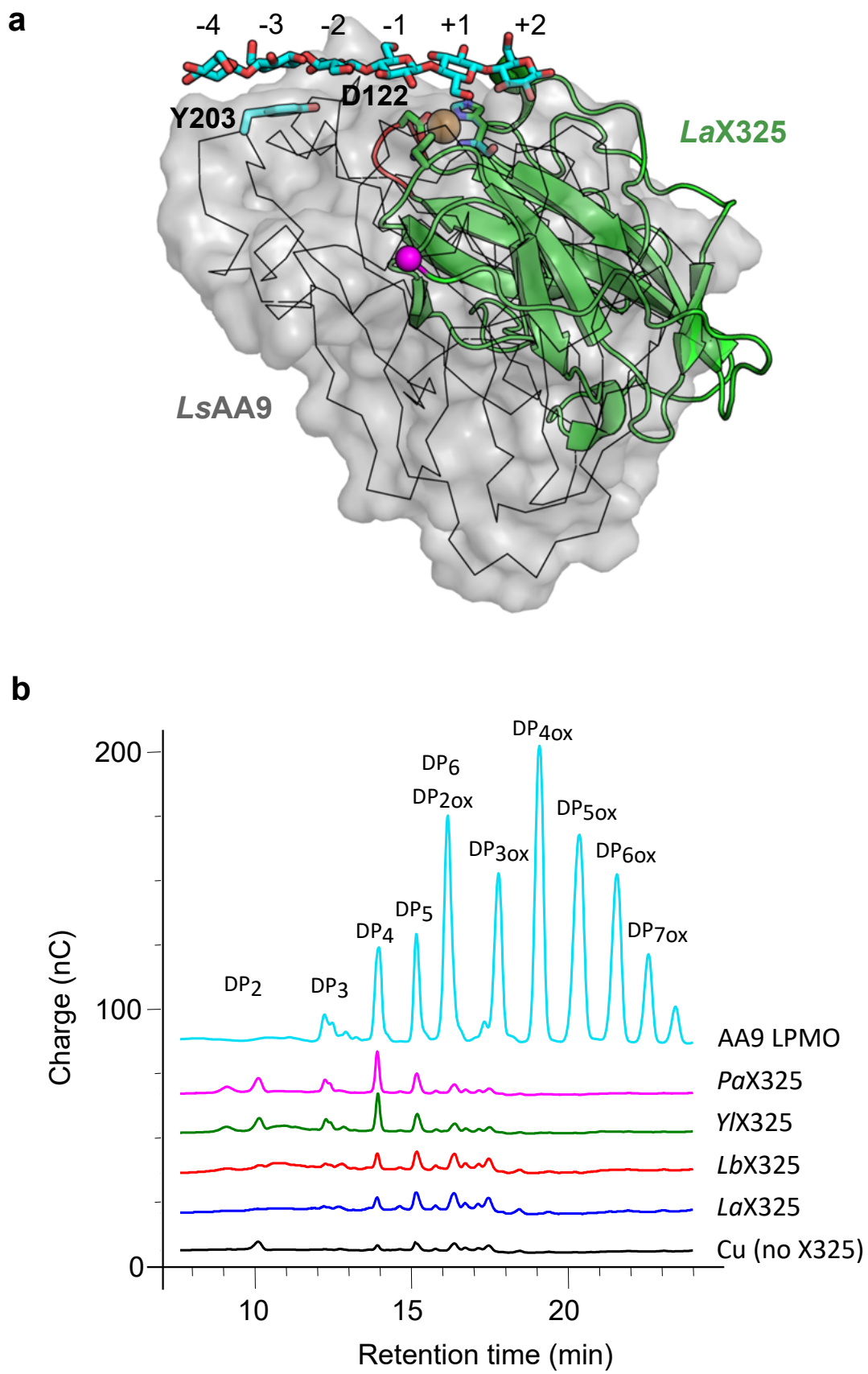
a
-4
-3
-2
-1
+1
+2
D122
Y203
LaX325
LsAA9
b
200
100
0
Charge (nC)
DP2
DP3
DP4
DP5
DP6
DP2ox
DP3ox
DP4ox
DP5ox
DP6ox
DP7ox
AA9 LPMO
PaX325
YlX325
LbX325
LaX325
Cu (no X325)
10
15
20
Retention time (min)

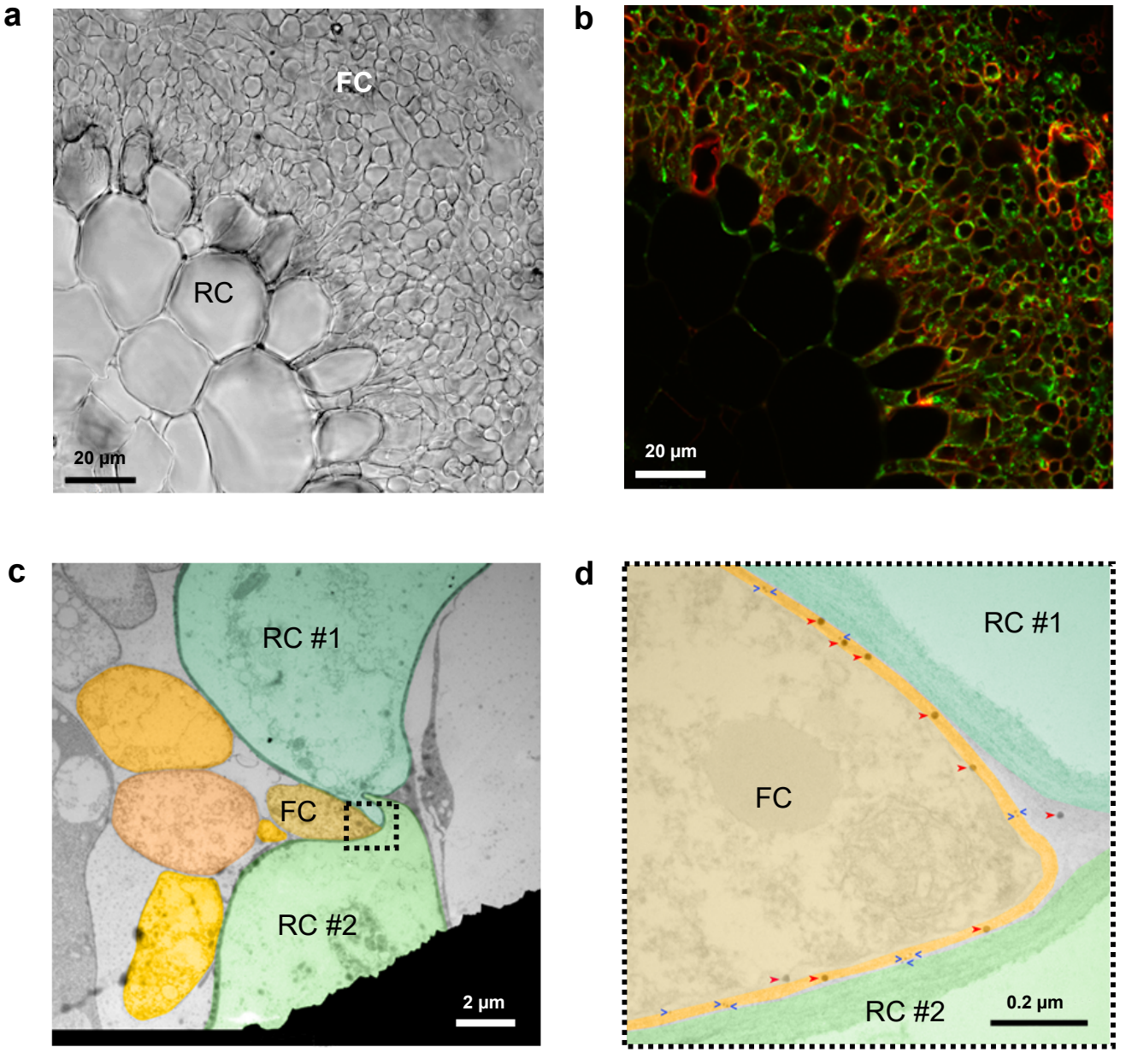
a
FC
RC
20 µm
b
20 µm
c
RC #1
FC
RC #2
2 µm
d
RC #1
FC
RC #2
0.2 µm

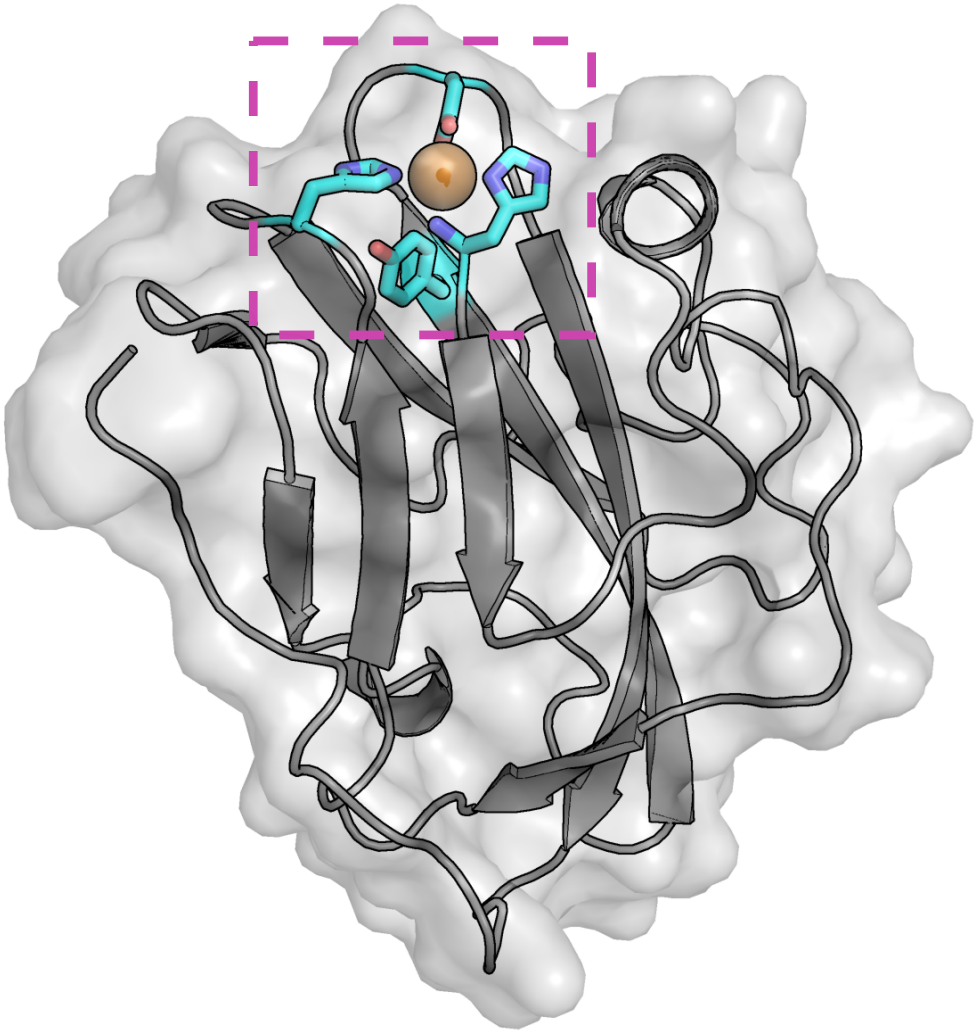

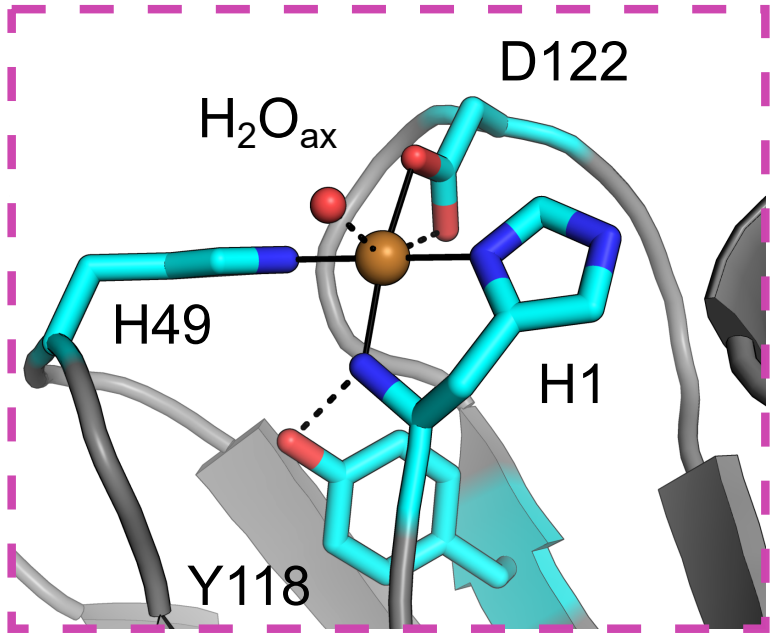
D122
H_2O_{ax}
H49
H1
Y118